[24] S. Ahmed, "Finite-element method for waveguide problems," *Electron. Lett.*, vol. 4, pp. 387–389, Sept. 1968.
[25] R. S. Martin and J. H. Wilkinson, "Reduction of the symmetric eigenproblem $Ax=\lambda Bx$ and related problems to standard form," *Numerische Mathematik*, vol. 11, pp. 99–110, 1968.
[26] D. G. Corr, "Finite difference analysis of hybrid modes in microstrip structures," Ph.D. dissertation, University of London, London, England, Aug. 1970.
[27] D. Gelder, "Numerical determination of microstrip properties using the transverse field components," *Proc. Inst. Elec. Eng.*, vol. 117, pp. 699–703, Apr. 1970.
[28] H. R. Schwartz, "Tridiagonalization of a symmetric band matrix," *Numerische Mathematik*, vol. 12, pp. 231–241, 1968.
[29] W. Barth, R. S. Martin, and J. H. Wilkinson, "Calculation of the eigenvalues of a symmetric tridiagonal matrix by the method of bisection," *Numerische Mathematik*, vol. 9, pp. 336–393, 1967.
[30] J. H. Wilkinson, "Calculation of the eigenvectors of a symmetric tridiagonal matrix by inverse interation," *Numerische Mathematik*, vol. 4, pp. 368–376, 1962.
[31] G. Peters and J. H. Wilkinson, "Eigenvalues of $Ax=\lambda Bx$ with band symmetric A and B," *Comput. J.*, vol. 12, pp. 398–404, 1969.
[32] R. E. Collin, *Field Theory of Guided Waves*. New York: McGraw-Hill, 1960.
[33] P. M. Morse and H. Feshbach, *Methods of Theoretical Physics*, vol. 2. New York: McGraw-Hill, 1953, p. 1477.
[34] R. F. Harrington, *Field Computation by Moment Methods*. New York: Macmillan, 1968, pp. 147–150.

Frequency-Dependent Characteristics of Microstrip Transmission Lines

MARK K. KRAGE AND GEORGE I. HADDAD

***Abstract*—A method for determining the frequency-dependent characteristics of both single and coupled lines in shielded microstrip is presented. Numerical results are given for a variety of dielectric configurations and the effects of geometry on the dispersion characteristics are examined in detail. Of particular interest are the characteristics of coupled lines on compensated dielectric structures, i.e., structures that are capable of achieving equal even- and odd-mode phase velocities, and the effects of dispersion on the directivity characteristics of such lines are discussed. In addition, the variation of impedance as a function of frequency, where the impedance is defined as the ratio of the power to the square of the longitudinal current, is presented for representative cases of single and coupled lines.**

I. Introduction

FOR sufficiently low frequencies the quasi-TEM theory can be employed to obtain the characteristics of microstrip lines and, using this approximation, extensive design data have been calculated for both single and coupled lines [1]–[3]. When the wavelength in a microstrip line becomes comparable to the transverse dimensions of the line the deviation from quasi-TEM behavior becomes significant and higher order modes of propagation become possible. Recently, several authors [4]–[10] have advanced methods for calculating the frequency-dependent characteristics of microstrip lines, but only limited numerical results have been presented for both open and shielded microstrip configurations. Most authors have confined their attention to the dominant mode characteristics of single lines, but Denlinger [9] and Gelder [10] have considered the characteristics of a pair of coupled lines and Mittra and Itoh [7] and Pregla and Schlosser [11] have considered higher order modes in a shielded structure.

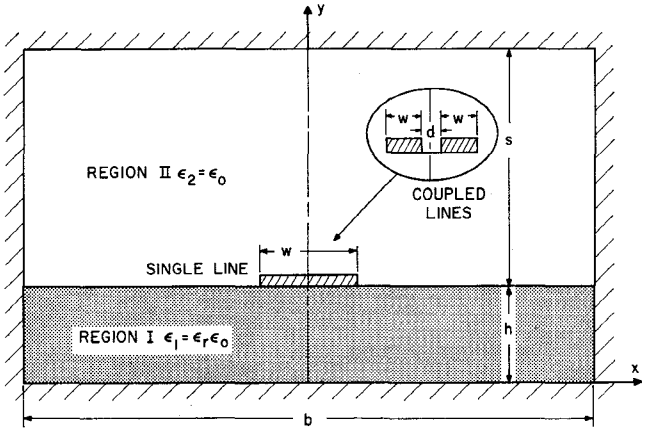

Fig. 1. Shielded microstrip geometry.

In this paper a method is presented for calculating the frequency-dependent characteristics of shielded microstrip lines, and the effects of geometry on the dispersion characteristics of single and coupled lines are considered in detail. Although the analysis will be carried out only for the configuration of Fig. 1, results will be presented for the modified configurations of Figs. 2 and 3, as well as for the geometry of Fig. 1. It was demonstrated in a previous paper [3] that coupled lines on the modified geometries can achieve equal even- and odd-mode phase velocities and are therefore capable of achieving high

Manuscript received January 31, 1972; revised May 8, 1972. This work was supported by a grant from Omni Spectra, Inc., Farmington, Mich.

M. K. Krage was with the Electron Physics Laboratory, Department of Electrical and Computer Engineering, University of Michigan, Ann Arbor, Mich. 48104. He is now with the General Motors Research Laboratories, Warren, Mich.

G. I. Haddad is with the Electron Physics Laboratory, Department of Electrical and Computer Engineering, University of Michigan, Ann Arbor, Mich. 48104.

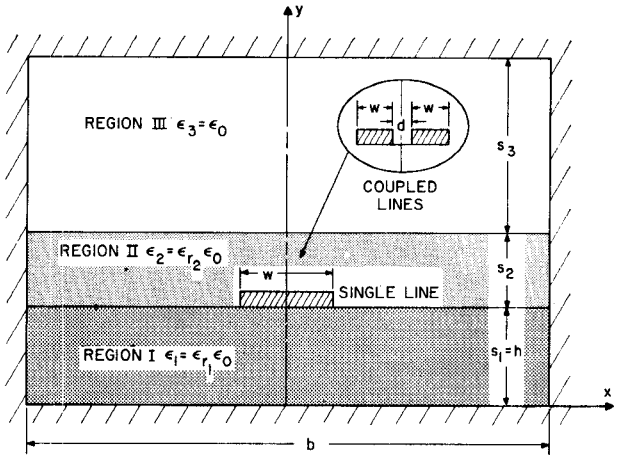

Fig. 2. Overlay-shielded microstrip.

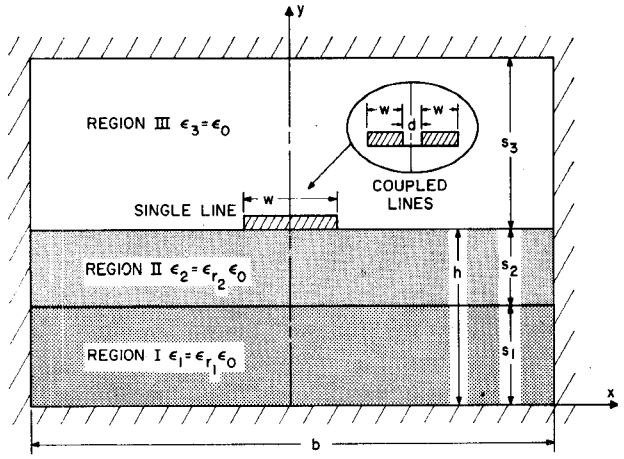

Fig. 3. Composite-substrate-shielded microstrip.

directivities. The effects of dispersion on the directivity characteristics of these lines will be considered. In addition, the variation of impedance with frequency, where the impedance is defined as the ratio of the power to the square of the longitudinal current, is presented for representative cases of both single and coupled lines.

II. Formulation of the Method

The cross-sectional geometry for the shielded microstrip that will be analyzed is shown in Fig. 1. The transmission line consists of a perfectly conducting strip of zero thickness and finite width residing on top of a dielectric substrate which, in turn, is enclosed inside a perfectly conducting box. The structure is divided into two regions, corresponding to the air and dielectric regions of the structure, and the wave equations for each region are given by

$$(\nabla^2 + k_1^2)\begin{Bmatrix}\overline{E}_1\\ \overline{H}_1\end{Bmatrix} = 0, \qquad \text{for } y < h \tag{1}$$

$$(\nabla^2 + k_2^2)\begin{Bmatrix}\overline{E}_2\\ \overline{H}_2\end{Bmatrix} = 0, \qquad \text{for } y > h \tag{2}$$

where an $e^{j\omega t}$ time variation is assumed and $k_i^2 = \omega^2\mu_0\epsilon_0\epsilon_{r_i}$ $(i=1, 2)$. Since the transverse-field components can be determined from the longitudinal-field components by the relations

$$(k_i^2 + \gamma^2)E_{xi} = -j\omega\mu_0\frac{\partial H_{zi}}{\partial y} + \gamma\frac{\partial E_{zi}}{\partial x} \tag{3}$$

$$(k_i^2 + \gamma^2)H_{xi} = j\omega\epsilon_i\frac{\partial E_{zi}}{\partial y} + \gamma\frac{\partial H_{zi}}{\partial x} \tag{4}$$

$$(k_i^2 + \gamma^2)E_{yi} = j\omega\mu_0\frac{\partial H_{zi}}{\partial x} + \gamma\frac{\partial E_{zi}}{\partial y} \tag{5}$$

$$(k_i^2 + \gamma^2)H_{yi} = -j\omega\epsilon_i\frac{\partial E_{zi}}{\partial x} + \gamma\frac{\partial H_{zi}}{\partial y} \tag{6}$$

where an $e^{\gamma z}$ variation is assumed; it is sufficient to consider only the longitudinal $(-z)$ components of the fields in (1).

The various modes in microstrip can be considered in terms of even E_z-odd H_z and odd E_z-even H_z field configurations; for simplicity, these modes will be referred to as the even and odd modes, respectively. The dominant mode on a single line is an even mode, while a pair of coupled lines can support one even and one odd dominant mode. Using the conditions that $E_z = E_x = 0$ on the topwall and ground plane and $E_z = E_y = 0$ on the sidewalls, the solutions for E_z and H_z for the $\begin{Bmatrix}\text{even}\\ \text{odd}\end{Bmatrix}$ modes can be written in the following form:

$$E_{z1}(x, y) = \sum_n \overline{A}_{1n}\frac{\sinh \beta_{1n}y}{\sinh \beta_{1n}h}\begin{Bmatrix}\cos \alpha_n x\\ \sin \alpha_n x\end{Bmatrix} \tag{7}$$

$$H_{z1}(x, y) = \sum_n \overline{B}_{1n}\frac{\cosh \beta_{1n}y}{\cosh \beta_{1n}h}\begin{Bmatrix}\sin \alpha_n x\\ \cos \alpha_n x\end{Bmatrix} \tag{8}$$

$$E_{z2}(x, y) = \sum_n \overline{A}_{2n}\frac{\sinh \beta_{2n}(s + h - y)}{\sinh \beta_{2n}s}\begin{Bmatrix}\cos \alpha_n x\\ \sin \alpha_n x\end{Bmatrix} \tag{9}$$

$$H_{z2}(x, y) = \sum_n \overline{B}_{2n}\frac{\cosh \beta_{2n}(s + h - y)}{\cosh \beta_{2n}s}\begin{Bmatrix}\sin \alpha_n x\\ \cos \alpha_n x\end{Bmatrix} \tag{10}$$

where

$$\alpha_n = \begin{Bmatrix}(2n + 1)\pi/b\\ 2n\pi/b\end{Bmatrix}$$

and β_{in} is constrained by the relation

$$-\alpha_n^2 + \beta_{in}^2 + \gamma^2 + k_i^2 = 0, \qquad \text{for } i = 1, 2. \tag{11}$$

The expansion coefficients for E_{zi} and H_{zi} can be related by the boundary conditions at the dielectric interface. These boundary conditions are written in terms of the surface current and surface charge densities on the strip(s), and are given by the relations

$$E_{z1}(x, h) = E_{z2}(x, h) \tag{12}$$

$$E_{x1}(x, h) = E_{x2}(x, h) \tag{13}$$

$$\epsilon_1 E_{y1}(x, h) = \epsilon_2 E_{y2}(x, h) - \rho_s(x) \tag{14}$$

$$H_{z1}(x, h) = H_{z2}(x, h) - K_x(x) \tag{15}$$

$$H_{x1}(x, h) = H_{x2}(x, h) + K_z(x) \tag{16}$$

$$H_{y1}(x, h) = H_{y2}(x, h) \tag{17}$$

where ρ_s, K_x, and K_z are the surface charge, transverse current, and longitudinal current densities, respectively, on the perfectly conducting strip(s).

Using the relations of (3)–(6), the boundary conditions at $y=h$ involving the transverse-field components can be written entirely in terms of the longitudinal-field components and the surface current densities.

With the following definitions:

$$K_x(x) = \sum_n \overline{K}_{xn} \sin \alpha_n x$$

$$K_z(x) = \sum_n \overline{K}_{zn} \cos \alpha_n x$$

$$\rho_s(x) = \sum_n \bar{\rho}_{sn} \cos \alpha_n x$$

and the relations of (7)–(10), the equations in E_{zi} and H_{zi} can be written entirely in terms of the corresponding Fourier expansions. Term-by-term comparison can then be used in solving (12)–(17) for A_{1n} and B_{1n}. Since the algebraic manipulations leading to the desired equations are similar to those presented by other authors, the intermediate steps have been omitted.

One result of interest is the continuity relation

$$\pm \alpha_n \overline{K}_{xn} + \gamma \overline{K}_{zn} + j\omega \bar{\rho}_{sn} = 0 \tag{18}$$

where the $\pm$ refers to the $\begin{Bmatrix} \text{even} \\ \text{odd} \end{Bmatrix}$ mode. It can be seen from this relation that K_x is $\pm 90°$ out of phase with $\overline{K}_{zn}$ and $\bar{\rho}_{sn}$ when γ is pure imaginary. In the subsequent equations, K_x is replaced by jK_x so that both $\overline{K}_{xn}$ and $\overline{K}_{zn}$ can be considered real. Upon elimination of $\bar{\rho}_{sn}$, the final expressions give a set of two equations in terms of $\overline{A}_{1n}$, $\overline{B}_{1n}$, $\overline{K}_{xn}$, and $\overline{K}_{zn}$, which are solved to obtain $\overline{A}_{1n}$ and $\overline{B}_{1n}$ in terms of $\overline{K}_{xn}$ and $\overline{K}_{zn}$ as follows:

$$\overline{A}_{1n} = \frac{j\omega\mu(\gamma^2+k_1^2)(\gamma^2+k_2^2)\{\pm[(\gamma^2+k_2^2)\beta_{1n}\tanh\beta_{1n}h + (\gamma^2+k_1^2)\beta_{2n}\coth\beta_{2n}s]\overline{K}_{zn} \pm j\alpha_n\gamma[\beta_{1n}\tanh\beta_{1n}h + \beta_{2n}\tanh\beta_{2n}s]\overline{K}_{xn}\}}{\{[k_1^2(\gamma^2+k_2^2)\beta_{1n}\coth\beta_{1n}h + k_2^2(\gamma^2+k_1^2)\beta_{2n}\coth\beta_{2n}s] \cdot [(\gamma^2+k_2^2)\beta_{1n}\tanh\beta_{1n}h + (\gamma^2+k_1^2)\beta_{2n}\tanh\beta_{2n}s] + \alpha_n^2\gamma^2(k_2^2-k_1^2)^2\}} \tag{19}$$

and

$$\overline{B}_{1n} = \frac{-(\gamma^2+k_1^2)[\pm(\gamma^2+k_2^2)(k_2^2-k_1^2)\alpha_n\gamma\overline{K}_{zn} + j\{(\alpha_n\gamma)^2(k_2^2-k_1^2) - \beta_{2n}\tanh\beta_{2n}s[k_1^2(\gamma^2+k_2^2)\beta_{1n}\coth\beta_{1n}s + k_2^2(\gamma^2+k_1^2)\beta_{2n}\coth\beta_{2n}s]\}\overline{K}_{xn}]}{\{[k_1^2(\gamma^2+k_2^2)\beta_{1n}\coth\beta_{1n}h + k_2^2(\gamma^2+k_1^2)\beta_{2n}\coth\beta_{2n}s] \cdot [(\gamma^2+k_2^2)\beta_{1n}\tanh\beta_{1n}h + (\gamma^2+k_1^2)\beta_{2n}\tanh\beta_{2n}s] + \alpha_n^2\gamma^2(k_2^2-k_1^2)^2\}} \cdot \tag{20}$$

The preceding set of relations gives two equations in four unknowns, and two additional boundary conditions are necessary for a solution. These conditions are given by the requirement that the tangential electric fields on the strip at $y=h$ are zero, i.e.,

$$E_z(x, h) = 0, \qquad \text{for } |x'| \leq w/2$$

and

$$E_x(x, h) = 0, \qquad \text{for } |x'| < w/2$$

where $x'=x$ for a single strip and $x'=x\pm(d/2+w/2)$ for coupled strips. Since $E_z(x, h)=0$ on the strip for all $|x'| \leqq w/2$, the condition that $E_x(x, h)=0$ for $|x'|<w/2$ is equivalent to requiring $(\partial H_z/\partial y)(x, h)=0$ for $|x'|<w/2$. The boundary conditions then become

$$\sum_{n=0}^{\infty} \overline{A}_{1n} \begin{Bmatrix} \cos \alpha_n x \\ \sin \alpha_n x \end{Bmatrix} = 0, \qquad \text{for } |x'| \leqq w/2 \tag{21}$$

and

$$\sum_{n=0}^{\infty} \beta_{1n} \tanh \beta_{1n} h \overline{B}_{1n} \begin{Bmatrix} \sin \alpha_n x \\ \cos \alpha_n x \end{Bmatrix} = 0, \qquad \text{for } |x'| < w/2 \tag{22}$$

where $\overline{A}_{1n}$ and $\overline{B}_{1n}$ are given in terms of the longitudinal and transverse current distributions by (19) and (20).

The longitudinal and transverse current distributions are absolutely integrable and continuous functions of x in the range $|x'|<w/2$, and therefore admit to expansions in terms of a complete set of basis functions on the interval $|x'| \leqq w/2$. When N_z and N_x terms are used in the expansions of the longitudinal and transverse current distributions, respectively, the N_z+N_x coefficients can be evaluated from N_z' and N_x' equations, where $N_z'+N_x'=N_z+N_x$, which require the z- and x-components, respectively, of the electric field to be zero on the strip. A set of such equations can be generated from (21) and (22) by requiring these equations to hold at equally spaced points on the strip. This set of homogeneous equations has a nontrivial solution if and only if the determinant of the coefficients is zero, and the value or values of the propagation constant are then determined by those values of γ for which the determinant is zero. When the determinant is zero, the coefficients of the current expansions can be evaluated from any set of N_z+N_x-1 equations by assuming a nonzero value for one of the coefficients, and any field related quantity can then be determined.

In some cases this procedure may fail to give a zero determinant where a root should occur. This situation arises when the current distribution is insufficient to produce zeros of the tangential electric fields at the required points on the strip. In such cases, however, it has been found that the determinant exhibits a sharp minimum in the vicinity of the expected value of the propagation constant and that the current distribution, obtained from solving N_z+N_x-1 of the equations that

gave the minimum determinant, is usually quite reasonable.

In another case, a zero-order spurious solution can occur for a particular choice of N_z and N_x in the vicinity of $\bar{\gamma}^2 \triangleq |\gamma/k_0|^2 = (\epsilon_r+1)/2$. In this case, however, determinants of both higher order and lower order give neither a zero nor a minimum in the vicinity of the spurious root, and inspection of the determinant elements that give the spurious solution revealing that several of the elements may simultaneously be zero and, as a result, give a trivial solution. It should be noted that Daly [4] has encountered a similar problem near $\bar{\gamma}^2 = (\epsilon_r+1)/2$ in his formulation of the problem, but he attributes this zero to a zero-order surface-wave mode. His solution for the resulting field pattern, however, shows violent oscillations in the longitudinal magnetic field, and this is indicative of the possibility of a trivial solution. Also the occurrence of two zero-order modes is an unobserved phenomenon, and it is concluded that the root near $\bar{\gamma}^2 = (\epsilon_r+1)/2$ must indeed be a spurious root.

The dominant mode for a single microstrip transmission line is an even mode, and the longitudinal and transverse current distributions are then even and odd functions, respectively, of the x-coordinate. The longitudinal current distributions for this mode can therefore be expanded in a Legendre polynomial series of the form

$$K_z(x) = \sum_{n=0}^{\infty} C_n P_{2n}(x/a), \qquad \text{for } |x| \leqq a$$
$$K_z(x) \equiv 0, \qquad \text{for } |x| > a \tag{23}$$

where $a = w/2$ and the $P_{2n}(x)$ are the even Legendre polynomials.

The continuity of H_z at the edges of the strip requires the transverse current to be zero at the strip edges, and the transverse current distribution then has a sine expansion of the form

$$K_x(x) = \sum_{n=1}^{\infty} D_n \sin \frac{n\pi x}{a}, \qquad \text{for } |x| \leqq a$$
$$K_x(x) \equiv 0, \qquad \text{for } |x| \geqq a. \tag{24}$$

An odd-mode excitation is also possible on a single line (e.g., the Shafer mode [12]), and for this case the longitudinal and transverse current distributions would be of the form

$$K_z(x) = \sum_{n=1}^{\infty} C_n P_{2n-1}\left(\frac{x}{a}\right)$$
$$K_x(x) = \sum_{n=1}^{\infty} D_n \sin\left[(2n-1)\frac{(x+a)}{2a}\right]. \tag{25}$$

The odd-mode excitation for a single line, however, has not been considered.

The analysis can be extended to the case of two coupled microstrip lines through modification of the current distributions. In this case there are two zero-order modes corresponding to the even- and odd-mode excitations of the lines. In either case the current distributions on one of the strips is neither symmetric nor antisymmetric, and the distributions on one of the strips are of the form

$$K_z(x) = \sum_{n=0}^{N_z} C_n P_n\left(\frac{x - d/2 - a}{a}\right) \tag{26a}$$

$$K_x(x) = \sum_{n=1}^{N_x} D_n \sin n\pi\left(\frac{x - d/2}{2a}\right), \qquad \text{for } d/2 \leqq x \leqq d/2 + 2a \tag{26b}$$

$$K_x(x) = K_z(x) \equiv 0, \qquad \text{for } 0 \leqq x < d/2 + 2a < x < \infty \tag{26c}$$

where d is the separation between the strips, $P_n(x)$ are the Legendre polynomials, $a = w/2$, and w is the width of the strip. The even-mode excitation will again correspond to the even E_z-odd H_z field configuration, while the odd-mode excitation again corresponds to the odd E_z-even H_z field configuration.

Using the preceding current distributions for single and coupled lines, the phase velocity characteristics were determined by finding those values of the propagation constants that give a zero value for the determinant at a particular frequency. The determinant roots were found by iteration on γ and were located within one part in 10^6. In general, this procedure generates the phase-velocity characteristics of both dominant and higher order modes but, due to a lack of space, the higher order mode characteristics will not be considered. A more complete discussion of the results using the method of this paper, including higher order modes for both open and shielded microstrip, as well as experimental results for compensated dielectric couplers, is given in [13]. Also the low-frequency calculations for large box dimensions have shown agreement with the data of Bryant and Weiss [2] to better than 1 percent for the effective dielectric constants of both single and coupled lines over a wide range of dimensions. In the case of single lines, the agreement for $\epsilon_r = 10$ was better than 1 percent for all w/h in the range $0.2 \leqq w/h \leqq 1.5$ when $N_z = 3$ and $N_x = 1$ were used in the current distributions. Similarly, the agreement was within 1 percent for all coupled-line cases considered when $N_z = 5$ and $N_x = 1$ were used in the current distributions. The frequency-dependent characteristics of these lines are presented in the following section. In general, the computer time for the calculation of the propagation constant and impedance at a single frequency is of the order of 15 to 20 s on an IBM 360 computer when $N_z = 3$ and $N_x = 1$.

III. Numerical Results for Shielded Microstrip

The dispersion characteristics of the dominant mode have been evaluated for a variety of geometries and these results are presented in this section. The phase velocity information is presented in terms of the effective dielectric constant, which is defined by $\epsilon_{reff} \triangleq \bar{\gamma}^2$

$= |\gamma/k_0|^2$, versus the normalized frequency hk_0, where $k_0 = 2\pi/\lambda_0$ and λ_0 is the free-space wavelength. In addition, the impedance characteristics as a function of frequency are presented for several representative cases.

The impedance is defined by the relation

$$Z_0 = 2\int_S \frac{P_z\, dxdy}{(I_z)^2} \tag{27}$$

where $P_z = (E \times H^*) \cdot \hat{z}$ is the magnitude of the Poynting vector in the direction of propagation, s is the cross-sectional surface enclosed by the metal walls, and I_z is the average value of the longitudinal current, i.e., $I_z = \int_{-a}^{a} K_z(x)\ dx$. Now, $(E \times H^*) \cdot \hat{z} = E_x H_y^* - E_y H_x^*$, and in region i with dielectric constant ϵ_{r_i} the z-component of the Poynting vector becomes

$$P_{zi} = \frac{1}{k_0^2(\epsilon_{ri} - \bar{\gamma}^2)}\left[\left(\bar{\gamma}\frac{\partial E_{zi}}{\partial x} + \eta\frac{\partial H_{zi}}{\partial y}\right)\cdot\left(\frac{\epsilon_{ri}}{\eta}\frac{\partial E_{zi}^*}{\partial x} + \bar{\gamma}\frac{\partial H_{zi}^*}{\partial y}\right) + \left(\bar{\gamma}\frac{\partial E_{zi}}{\partial y} - \eta\frac{\partial H_{zi}}{\partial x}\right)\cdot\left(\frac{\epsilon_{ri}}{\eta}\frac{\partial E_{zi}^*}{\partial y} - \bar{\gamma}\frac{\partial H_{zi}^*}{\partial x}\right)\right] \tag{28}$$

where $\eta = \sqrt{\mu_0/\epsilon_0}$.

The preceding equation can be simplified somewhat by noting that

$$\frac{\partial E_{zi}}{\partial x}\frac{\partial H_{zi}^*}{\partial y} = \frac{\partial E_{zi}^*}{\partial x}\frac{\partial H_{zi}}{\partial y}$$

and

$$\frac{\partial E_{zi}}{\partial y}\frac{\partial H_{zi}^*}{\partial x} = \frac{\partial E_{zi}^*}{\partial y}\frac{\partial H_{zi}}{\partial x}$$

or that

$$P_{zi} = \frac{1}{k_0^2(\epsilon_{ri} - \bar{\gamma}^2)}\left\{\frac{\bar{\gamma}\epsilon_{ri}}{\eta}\left[\left|\frac{\partial E_{zi}}{\partial x}\right|^2 + \left|\frac{\partial E_{zi}}{\partial y}\right|^2\right] + \eta\bar{\gamma}\left[\left|\frac{\partial H_{zi}}{\partial x}\right|^2 + \left|\frac{\partial H_{zi}}{\partial y}\right|^2\right] + (\bar{\gamma}^2 + \epsilon_{ri})\left(\frac{\partial E_{zi}}{\partial x}\frac{\partial H_{zi}^*}{\partial y} - \frac{\partial E_{zi}}{\partial y}\frac{\partial H_{zi}^*}{\partial x}\right)\right\}. \tag{29}$$

For the bulk of the following results, a Legendre polynomial expansion is used for the longitudinal current distribution and a sine expansion is used for the transverse current distribution. For single lines, three terms were used in the longitudinal expansion ($N_z = 3$) and one term was used in the transverse expansion ($N_x = 1$). Higher order expansions with $N_z = 4$ and 5 and $N_x = 2$ have also been used for single lines with little apparent increase in accuracy, i.e., the value of γ changes by less than 0.5 percent and the impedance changes by less than 0.1 percent.

The results for the dispersion characteristics of single lines are given in Figs. 4 through 7. In Fig. 4 the dispersion characteristics are shown for three w/h ratios, and the change in the values of the effective dielectric constants from $hk_0 = 0$ to $hk_0 = 0.14$ are 5.1, 7.4, and 8.5 percent for w/h values of 0.2, 0.6, and 1.0, respectively. It is therefore seen that wide lines are more dispersive than narrow lines. Also shown in Fig. 4 are two experimentally determined curves [8], [14] for open microstrip with $w/h \approx 1$ and $\epsilon_r \approx 10$. When the effect of the topwall and the slightly different dielectric constants and linewidths are taken into account, the agreement with the calculated $w/h = 1.0$ curve is very good. In Fig. 5, the effect of the topwall on the effective dielectric constant is examined, and it is shown that the topwall effect can only be ignored when the ratio of the topwall spacing s to the thickness of the dielectric h is greater than 10. This result is in agreement with a similar calculation by Zysman and Varon [8]. The effects of varying the topwall spacing and the sidewall spacing are shown in Fig.

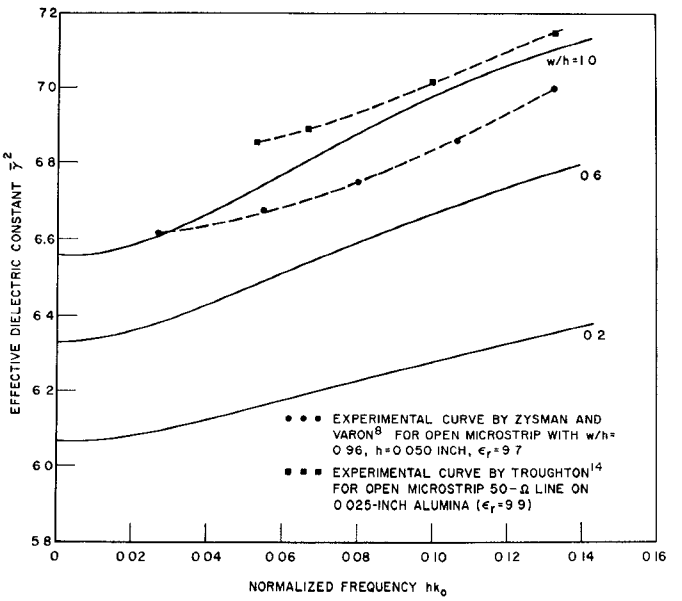

Fig. 4. Effective dielectric constant versus normalized frequency. ($\epsilon_r = 10$, $b/h = 20$, $s/h = 4$, $N_z = 3$, $N_x = 1$.)

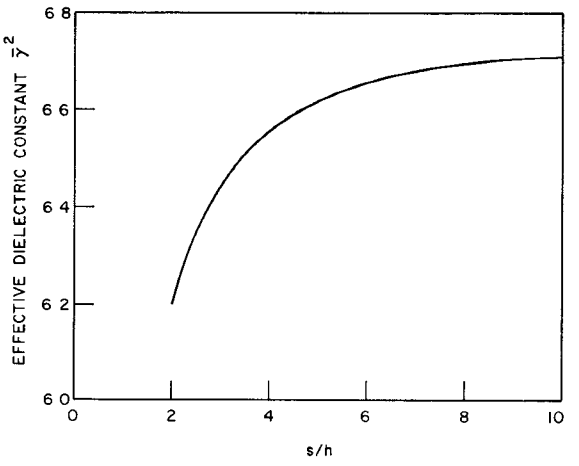

Fig. 5. Effective dielectric constant versus s/h. ($\epsilon_r = 10$, $w/h = 1$, $b/h = 20$, $hk_0 = 0.01$, $N_z = 3$, $N_x = 1$).

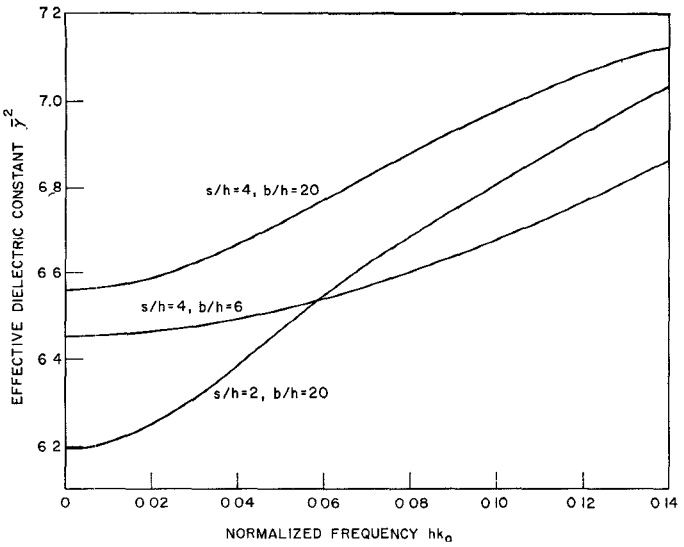

Fig. 6. Effective dielectric constant versus normalized frequency. ($\epsilon_r = 10$, $w/h = 1$, $N_z = 3$, $N_x = 1$.)

6. The results indicate that reducing the topwall spacing s increases the dispersion, while reducing the sidewall spacing b decreases the dispersion. In this case, the changes in the effective dielectric constant from $hk_0 = 0$ to 0.14 are 8.5 percent for $s/h = 4$ and $b/h = 20$, 12.2 percent for $s/h = 2$ and $b/h = 20$, and 6.5 percent for $s/h = 4$ and $b/h = 6$. The reduction in dispersion for reduced sidewall spacing can be related to the apparent lack of dispersion for the odd-mode characteristics of coupled lines. In the case of coupled lines, the sidewall effect for the odd mode is due to the electric wall between the strips, which is required by symmetry considerations. It is shown that the odd-mode characteristics display a virtual lack of dispersion for sufficiently small d_2/h, and that the dispersion increases as separation increases.

Finally, in Fig. 7, the dispersion characteristics of two different dielectrics, $\epsilon_r = 10$ and $\epsilon_r = 16$, and the characteristics of an overlay dielectric line are compared for a w/h value of 0.6. The changes in effective dielectric constant from $hk_0 = 0$ to $hk_0 = 0.14$ are 9.7 percent for $\epsilon_r = 16$, 7.4 percent for $\epsilon_r = 10$, and 6.2 percent for the overlay structure. It is therefore seen that, for the same stripwidth, the higher dielectric constant substrate exhibits more dispersion than lower dielectric-constant substrates, and that overlay dielectrics can be employed to further reduce the dispersion. On the basis of lines having the same low-frequency characteristic impedance the $\epsilon_r = 16$, $w/h = 0.6$ curve can be compared with the $\epsilon_r = 10$, $w/h = 1.0$ curve, since both lines have approximately the same zero-frequency 50-Ω characteristic impedance, with the result that the higher dielectric-constant substrate still exhibits more dispersion, i.e., 9.7 percent compared to 8.5 percent in the range of $hk_0 = 0$ to $hk_0 = 0.14$.

In the case of coupled lines, $N_z = 5$ and $N_x = 1$ were used in conjunction with the Legendre-sine current expansions in most calculations, and a comparison with

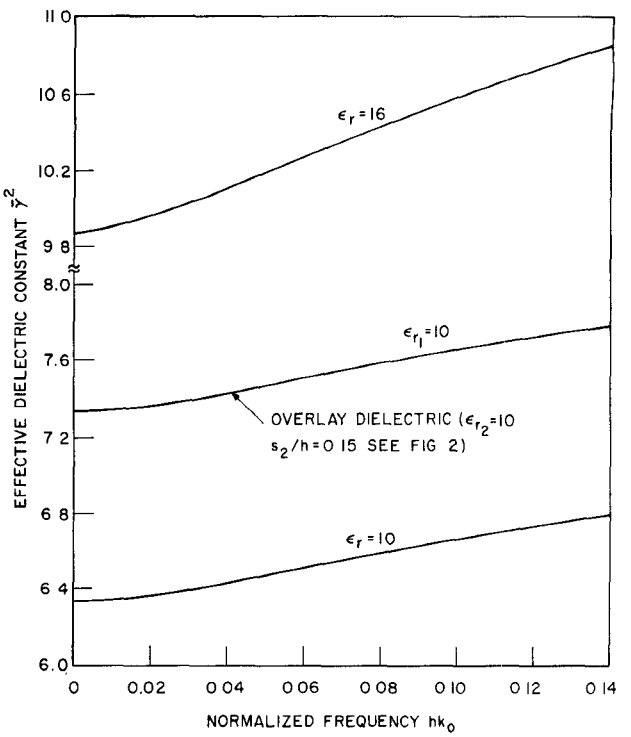

Fig. 7. Effective dielectric constant versus normalized frequency. ($w/h = 0.6$, $b/h = 20$, $s/h = 4$, $N_z = 3$, $N_x = 1$.)

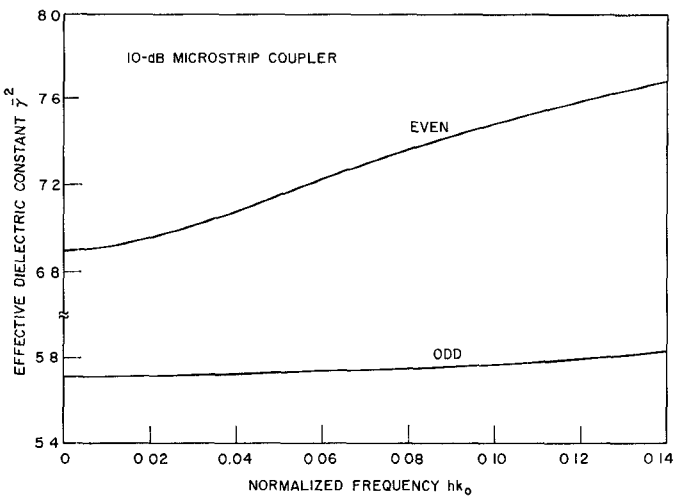

Fig. 8. Effective dielectric constant versus normalized frequency for the configuration of Fig. 1. ($\epsilon_r = 10$, $w/h = 0.85$, $d_2/h = 0.25$, $b/h = 20$, $s/h = 4$, $N_z = 5$, $N_x = 1$.)

$N_z = 3$ and $N_x = 1$ showed a change in the solution for $\tilde{\gamma}^2$ of the order of 1 percent, while increasing N_x to 2 with $N_z = 5$ showed a change of the order of 0.5 percent.

It should be noted that as N_x and N_z are increased, the solutions for $\tilde{\gamma}^2$ are generally confined to a very small range, and that the difference between successive orders of approximation decreases quite rapidly. From the observed convergence behavior, it is believed that the accuracy for the calculated values should be of the order of ± 1 percent.

In Fig. 8, the even- and odd-mode dispersion characteristics of a 10-dB directional coupler in the conven-

tional microstrip configuration are presented. As the results show, the odd-mode effective dielectric constant exhibits very little change, i.e., the change is only 1.9 percent at $hk_0 = 0.14$, while the even-mode characteristics show a change of 11.3 percent at $hk_0 = 0.14$. The more highly dispersive nature of the even mode can be related to the increase in dispersion as w/h increases since, for small separation, d_2/h, the field distribution of the two strips, will be approximately the same as a single strip of width $2w+d$.

If the frequency-dependent inductance and capacitance of a line are defined from the TEM relations $L = Z_0/v_p$ and $C = 1/Z_0 v_p$, the frequency-dependent capacitive and inductive coupling coefficients are then given by

$$k_L = \frac{\dfrac{Z_{0e}}{v_{pe}} - \dfrac{Z_{0o}}{v_{po}}}{\dfrac{Z_{0e}}{v_{pe}} + \dfrac{Z_{0o}}{v_{po}}} = \frac{1 - \dfrac{Z_{0o}}{Z_{0e}}\dfrac{v_{pe}}{v_{po}}}{1 + \dfrac{Z_{0o}}{Z_{0e}}\dfrac{v_{pe}}{v_{po}}}$$

$$= \frac{1 - \dfrac{Z_{0o}}{Z_{0e}}\left(\dfrac{\epsilon_{ro}}{\epsilon_{re}}\right)^{1/2}}{1 + \dfrac{Z_{0o}}{Z_{0e}}\left(\dfrac{\epsilon_{ro}}{\epsilon_{re}}\right)^{1/2}} \tag{30}$$

$$k_C = \frac{\dfrac{1}{Z_{0o}v_{po}} - \dfrac{1}{Z_{0e}v_{pe}}}{\dfrac{1}{Z_{0o}v_{po}} + \dfrac{1}{Z_{0o}v_{pe}}} = \frac{1 - \dfrac{Z_{0o}}{Z_{0e}}\left(\dfrac{\epsilon_{re}}{\epsilon_{ro}}\right)^{1/2}}{1 + \dfrac{Z_{0o}}{Z_{0e}}\left(\dfrac{\epsilon_{re}}{\epsilon_{ro}}\right)^{1/2}} \cdot \tag{31}$$

Assuming for the moment that Z_{0o}/Z_{0e} is independent of frequency, the behavior of ϵ_{re} and ϵ_{ro} in Fig. 8 indicates that k_L increases while k_C decreases with increasing frequency. The quasi-TEM results of a previous paper [3] indicated that, at zero frequency, the value of k_L is always greater than the value of k_C for this configuration, and since the directivity is proportional to $k_L - k_C$, the directivity should become worse at higher frequencies. It will be shown later that, at sufficiently high frequencies, the ratio of Z_{0o}/Z_{0e} decreases with increasing frequency, so that the increase in k_L will be greater than the corresponding decrease in k_C. The conclusion regarding the degradation of directivity with increasing frequency, however, will remain unchanged.

The preceding result further emphasizes the need for compensated dielectric structures to achieve high directivity couplers in microstrip. In Figs. 9 through 12, the dispersion characteristics of some compensated dielectric structures are presented. The method of analysis for these structures is essentially the same as the previous analysis and therefore is not presented. In Fig. 9, the even- and odd-mode dispersion characteristics are given for a 10-dB overlay structure, i.e., for the configuration of Fig. 2. In this case, the even- and odd-mode characteristics exhibit substantially less dispersion than the previous case, and at $hk_0 = 0.14$ the changes in the effective

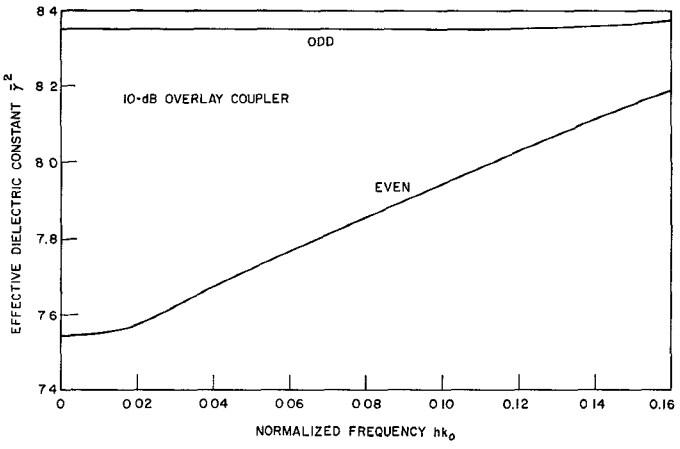

Fig. 9. Effective dielectric constant versus normalized frequency for the configuration of Fig. 2. ($\epsilon_{r_1} = 10$, $\epsilon_{r_2} = 10$, $w/h = 0.6$, $d_2/h = 0.2$, $b/h = 20$, $s_3/h = 4$, $s_2/h = 0.15$, $N_z = 5$, $N_x = 1$.)

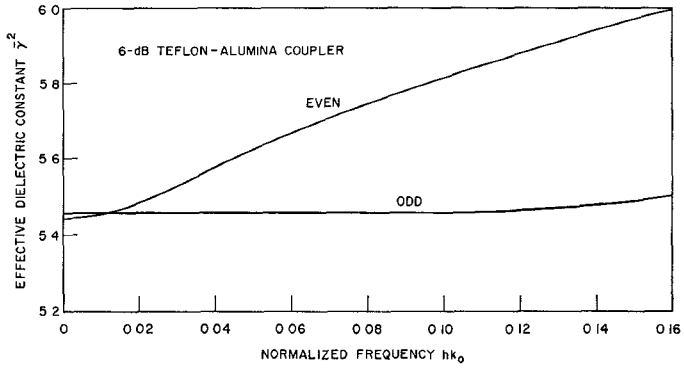

Fig. 10. Effective dielectric constant versus normalized frequenyc for the configuration of Fig. 3. ($\epsilon_{r_1} = 2.02$, $\epsilon_{r_2} = 10$, $w/h = 0.65$, $d_2/h = 0.045$, $b/h = 20$, $s_1/h = 0.1$, $s_2/h = 0.9$, $s_3/s_2 = 4$, $N_z = 5$, $N_x = 1$.)

dielectric constant from the zero-frequency values are 0.1 percent for the odd mode and 6.9 percent for the even mode. It is easily seen that the thickness of the overlay is too large to permit compensation [3] in the range of frequencies considered, and compensation will probably occur in the neighborhood of $hk_0 = 0.2$ or higher. Since both curves have asymptotes at $\bar{\gamma}^2 = 10$, there may exist a large range above the compensation point for which $\epsilon_{re} \approx \epsilon_{ro}$ or $k_L \approx k_C$. The excitation of higher order modes, however, may render this possibility impractical.

In Figs. 10 through 12, the dispersion characteristics of 6-dB, 10-dB, and 20-dB couplers utilizing the Teflon–alumina dielectric structure in the configuration of Fig. 3 are presented. The changes in the effective dielectric constants at $hk_0 = 0.14$ for the 6-dB coupler of Fig. 10 are 0.4 percent for the odd mode and 9.2 percent for the even one. It is noted that compensation in this case occurs at a relatively low frequency of $hk_0 \approx 0.01$. Due to the relatively small changes in ϵ_{re} and ϵ_{ro} in the vicinity of $hk_0 = 0.01$, a directional coupler with a midband frequency of $hk_0 = 0.01$ should behave essentially like a TEM directional coupler and should exhibit very high directivities over an octave bandwidth. However, if the compensation point were changed to a higher frequency,

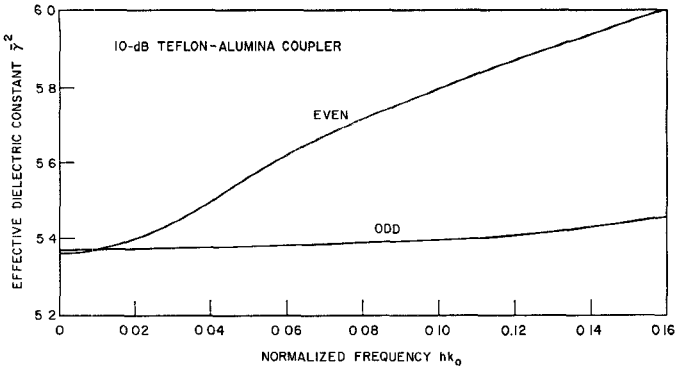

Fig. 11. Effective dielectric constant versus normalized frequency for the configuration of Fig. 3. ($\epsilon_{r_1}=2.02$, $\epsilon_{r_2}=10$, $w/h=0.88$, $d_2/h=0.29$, $b/h=20$, $s_1/h=0.11$, $s_2/h=0.89$, $s_3/s_2=4$, $N_z=5$, $N_x=1$.)

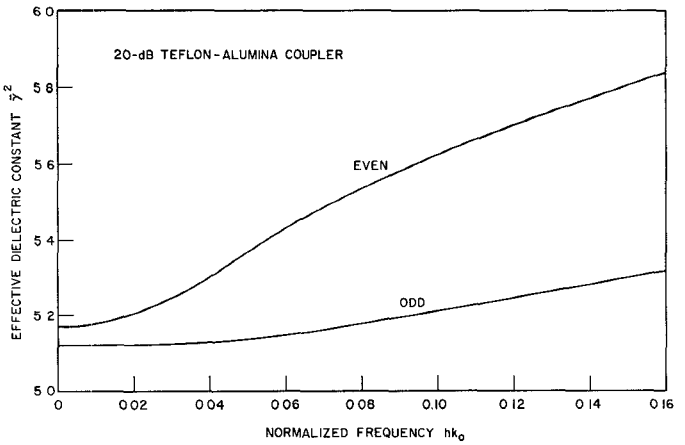

Fig. 12. Effective dielectric constant versus normalized frequency for the configuration of Fig. 3. ($\epsilon_{r_1}=2.02$, $\epsilon_{r_2}=10$, $w/h=1.15$, $d_2/h=1.34$, $b/h=20$, $s_1/h=0.14$, $s_2/h=0.86$, $s_3/s_2=4$, $N_z=5$, $N_x=1$.)

say $hk_0=0.1$, the change in ϵ_{re} would be much larger than in the previous case considered, and the minimum directivity would be much lower. Still, the directivity for this configuration should be substantially higher than for the conventional microstrip configuration.

The dispersion characteristics for the 10-dB Teflon–alumina coupler are shown in Fig. 11. The changes in the effective dielectric constants at $hk_0=0.14$ are 1 percent for the odd mode and 10.8 percent for the even mode, and again compensation occurs in the neighborhood of $hk_0=0.01$. It is noted that the dispersion for this 10-dB case is greater than for the 6-dB case, and that the 10-dB Teflon–alumina curves exhibit more dispersion than the 10-dB overlay coupler, but less dispersion than the conventional 10-dB coupler.

The even- and odd-mode dispersion characteristics for a 20-dB Teflon–alumina coupler are presented in Fig. 12. Since the coupling is relatively weak, the coupled lines should behave somewhat like two single lines. The changes in the effective dielectric constants at $hk_0=0.14$ are 3.1 percent for the odd mode and 12.9 percent for the even mode. Note that ϵ_{re} is greater than ϵ_{ro} at $hk_0=0$ so that compensation was not achieved. It is also noted that the difference between the relative changes in ϵ_{re} and ϵ_{ro} at $hk_0=0.14$ are nearly the same for the 6-dB,

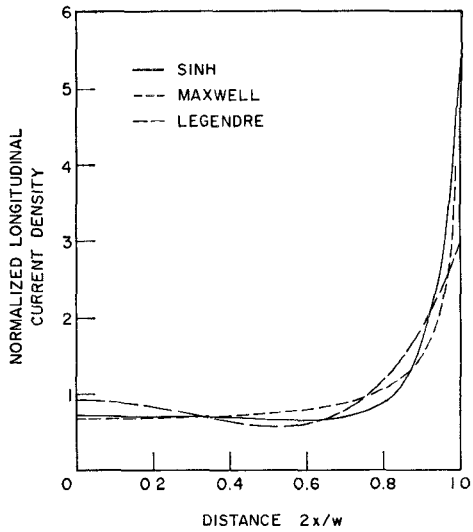

Fig. 13. Longitudinal current density versus distance for the configuration of Fig. 1. ($\epsilon_r=10$, $w/h=1$, $s/h=4$, $b/h=20$, $N_z=3$, $N_x=1$, $hk_0=0.01$.)

10-dB, and 20-dB couplers. However, the directivity is proportional to $(k_L-k_C)/(k_L+k_C)$ and, since (k_L+k_C) is less for weaker coupling values, the corresponding band-edge directivities in an octave bandwidth should be worse for the weak coupling situations. Assuming Z_{0e}/Z_{0o} does not change as a function of frequency, the minimum directivities of the 6-, 10-, and 20-dB couplers should be of the order of 41 dB, 30 dB, and 16 dB, respectively, over an octave bandwidth centered about $hk_0=0.08$. (This would correspond to a 4- to 8-GHz coupler when $h=0.025$ in.) If the compensation point is shifted to a lower value of hk_0, the minimum directivity over an octave bandwidth can be substantially increased. For a particular frequency range, the value of hk_0 can be reduced by using thinner substrates, but power handling limitations, losses, and fabrication techniques will, in general, place a lower limit on the substrate thickness.

The impedance as a function of frequency and the current distribution have been calculated for several representative cases, and the results for single lines are given in Figs. 13 through 15. The bulk of the impedance calculations have been made using a slightly different longitudinal current distribution approximation given by

$$K_z(x) = C_0 + \sum_{n=1}^{N_z} C_n \frac{\sinh 2n\pi x'/w}{\sinh n\pi}$$

for coupled strips and

$$K_z(x) = C_0 + \sum_{n=1}^{N_z} C_n \frac{\cosh 4n\pi x/w}{\cosh 2n\pi}$$

for single strips. The reason for this choice of distribution is primarily aesthetic, and a comparison of the solutions for the current distributions at $hk_0=0.01$ using Legendre polynomials and sinh functions are shown in Fig. 13. Also shown is the Maxwell distribution used by

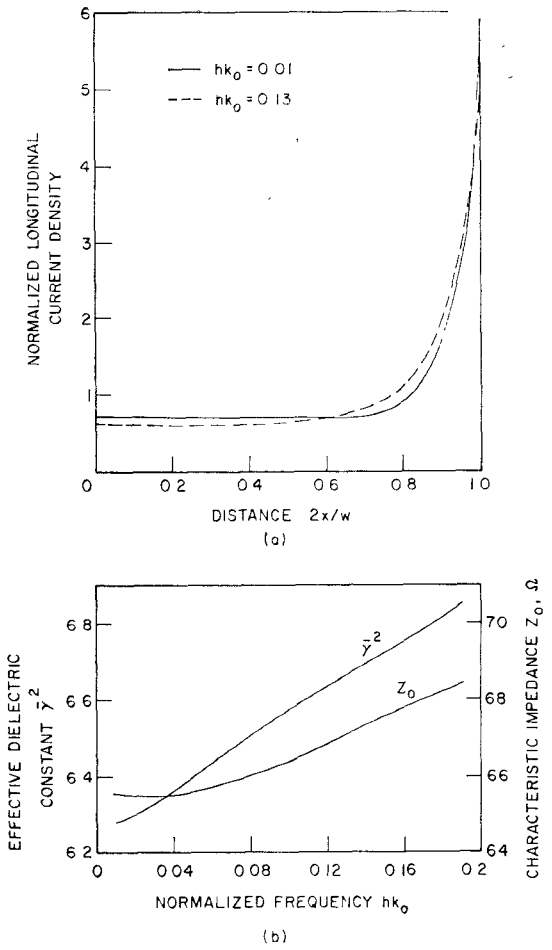

Fig. 14. Characteristics of a single line for the configuration of Fig. 1. (a) Normalized current density versus distance. (b) Effective dielectric constant and characteristic impedance versus normalized frequency. ($\epsilon_r = 10$, $w/h = 0.5$, $s/h = 4$, $b/h = 20$, $N_z = 3$, $N_x = 1$.)

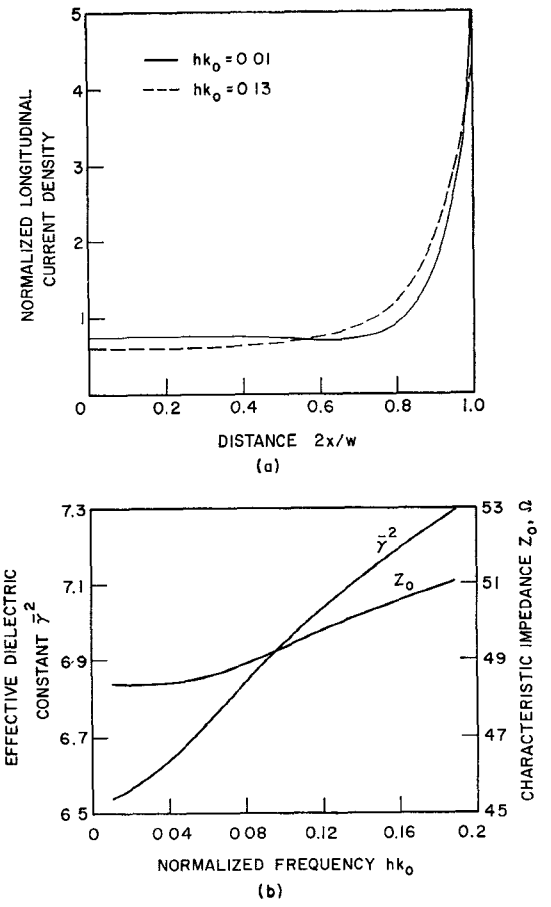

Fig. 15. Characteristics of a single line for the configuration of Fig. 1. (a) Normalized current density versus distance. (b) Effective dielectric constant and characteristic impedance versus normalized frequency. ($\epsilon_r = 10$, $w/h = 1$, $s/h = 4$, $b/h = 20$, $N_z = 3$, $N_x = 1$.)

Denlinger [5]. All the distributions are normalized such that $w^{-1}\int_{-w/2}^{w/2} K_z(x)\, dx = 1$. It can be seen from these curves that the polynomial distribution shows more oscillation than the sinh distribution and that its magnitude is not nearly as large at $x = w/2$. It is also observed that the sinh distribution and the Maxwell distribution are quite similar. The sinh distribution, therefore, looks more like the expected distribution at low frequencies, but in terms of the calculated values of $\bar{\gamma}$ or Z_0 the choice of distribution makes little apparent difference. The choice of the basis set for the longitudinal current distribution, however, does affect the solution for the transverse current distribution. It is found that the magnitude of the maximum value of K_x is somewhat smaller when the sinh distribution is employed, and it is believed that this result is related to the different shapes of the $K_z(x)$ distributions near $x = \pm w/4$. In both cases the magnitude of K_x is increasing as a function of frequency and is at least two orders of magnitude less than the average value of $K_z(x)$ at the highest frequency considered.

In Figs. 14 and 15 the longitudinal current distributions at $hk_0 = 0.01$ and 0.13, and the frequency dependence of the characteristic impedance and the effective dielectric constant are given for w/h values of 0.5 and 1. In both cases, the characteristic impedance initially decreases and then increases with increasing frequency, while the effective dielectric constant increases monotonically with increasing frequency. The change in impedance from $hk_0 = 0.01$ to $hk_0 = 0.19$ is 4.6 percent for $w/h = 0.5$ and 5.4 percent for $w/h = 1$, while the change in effective dielectric constant is 8 percent for $w/h = 0.5$, and 11.8 percent for $w/h = 1$. The impedance, therefore, changes more slowly than the effective dielectric constant as a function of frequency. The longitudinal current distribution also changes slightly as a function of frequency, and it appears that more current is concentrated at the edges of the strip at higher frequencies. The current distribution curves for values of hk_0 between 0.01 and 0.13 lie intermediate to the two curves shown, while the curves for hk_0 between 0.13 and 0.19 are virtually identical. It is also noted that distribution curves at $hk_0 = 0.01$ are nearly identical for w/h values of 0.5 and 1.

The frequency dependence of the impedance has also been considered by Denlinger [5] and Napoli and

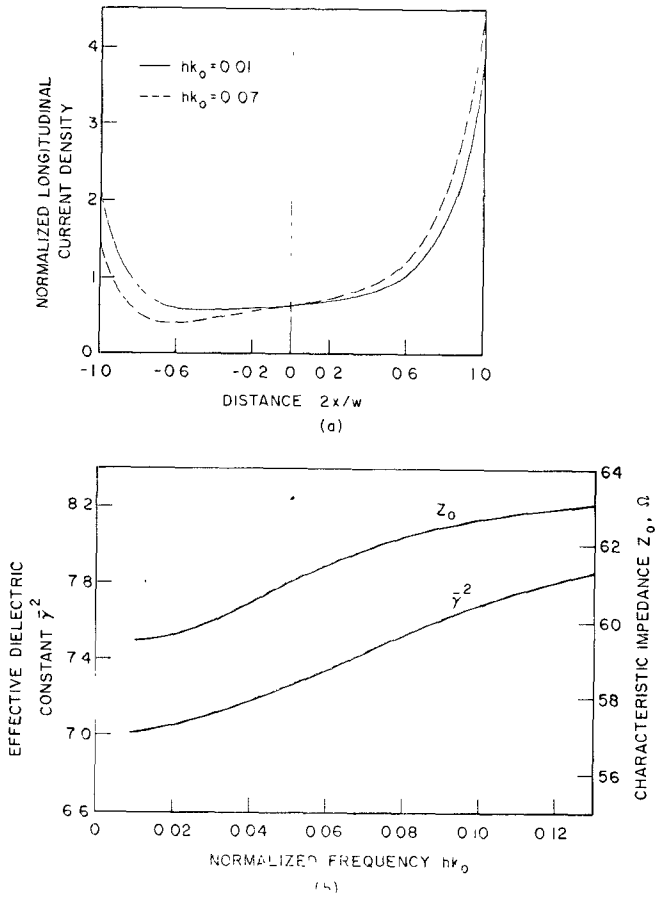

Fig. 16. Even-mode characteristics of a pair of coupled lines. (a) Normalized current density versus distance. (b) Effective dielectric constant and characteristic impedance versus normalized frequency. ($\epsilon_r = 10$, $w/h = 1$, $d_2/h = 0.4$, $s/h = 4$, $b/h = 20$, $N_s = 3$, $N_x = 1$, Fig. 1 configuration.)

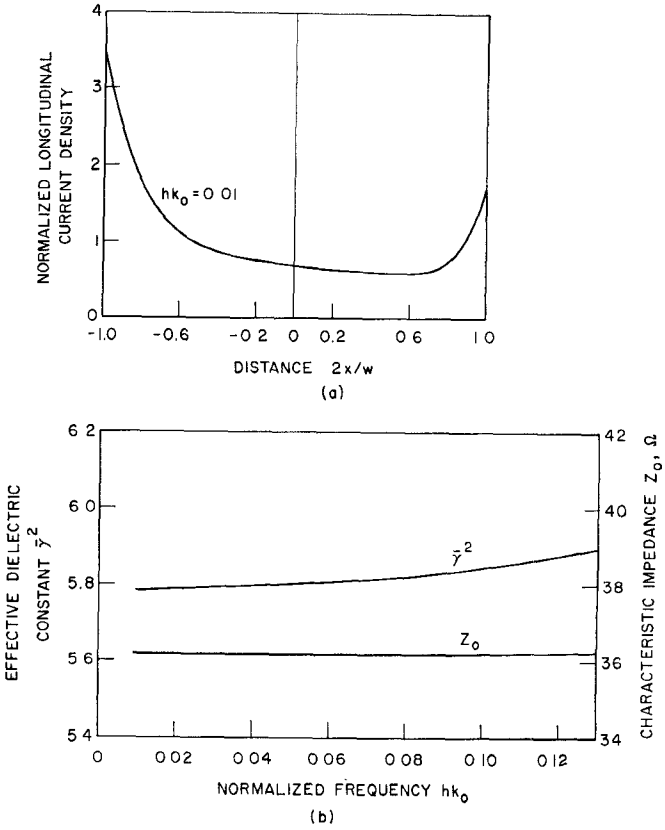

Fig. 17. Odd-mode characteristics of a pair of coupled lines. (a) Normalized current density versus distance. (b) Effective dielectric constant and characteristic impedance versus normalized frequency. ($\epsilon_r = 10$, $w/h = 1$, $d_2/h = 0.4$, $s/h = 4$, $b/h = 20$, $N_s = 3$, $N_x = 1$, Fig. 1 configuration.)

Hughes [15], but their conclusions are not in agreement with the preceding results. On the basis of a quasi-TEM model, Denlinger calculated a microstrip impedance from the relation $Z_0 = Z_0' \sqrt{\epsilon_{reff}}/\bar{\gamma}$, where Z_0' and ϵ_{reff} are calculated from the quasi-TEM theory. Since $\bar{\gamma}$ increases monotonically with frequency, this impedance decreases monotonically with increasing frequency. This value of impedance, however, is no better than the quasi-TEM value, since it does not relate the relative magnitudes of the electric and magnetic fields or the power to the current except at zero frequency. Napoli and Hughes, on the other hand, have attempted to measure the microstrip impedance relative to a TEM reference line, and they conclude that the impedance decreases more rapidly than the effective dielectric constant increases. Since the power and the longitudinal current should be continuous across the interface between the TEM line and the microstrip line, the measurements of Napoli and Hughes should be in agreement with the power–current impedance calculations. However, an examination of their data reveals that they have made various assumptions regarding the phases of the reflected signals. When these assumptions are removed, the data of Napoli and Hughes give a range of possible impedance values, and the calculated values of impedance then lie well within the predicted range. It should also be noted in this regard that standing-wave measurements in a TEM reference line of a 1-in long 50-Ω (zero-frequency) microstrip line (alumina substrate) terminated in a 50-Ω load show that the VSWR increases slowly with frequency, with a maximum VSWR of 1.2 up to 15 GHz [16]. The maximum VSWR for the impedance variation of Fig. 15(b), excluding mismatch due to the connectors and the load, would be of the order of 1.06. The impedance calculations, therefore, are in good agreement with the experimental data.

The longitudinal current distribution, impedance, and effective dielectric constant have also been calculated for a pair of coupled lines, and the corresponding even- and odd-mode characteristics are given in Figs. 16 and 17, respectively. The changes in the impedance and the effective dielectric constant at $hk_0 = 0.12$ from their zero-frequency values are 5.8 percent and 11.3 percent for the even mode and 0 percent and 1.7 percent for the odd mode, respectively. The values of k_L and k_C are $k_L = 0.29$ and $k_C = 0.20$ at $hk_0 = 0.01$, and $k_L = 0.333$ and $k_C = 0.21$ at $hk_0 = 0.12$, so that $(k_L - k_C)/(k_L + k_C)$ equals 0.184 at $hk_0 = 0.01$ and 0.226 at $hk_0 = 0.12$, respectively.

The corresponding directional couplers with midband frequencies of $hk_0 = 0.01$ and 0.12 would then have midband directivities of the order of 7 dB and 5.5 dB, respectively. The current distribution for the even mode is shown for two values of hk_0. As was found for the single strip, the current tends to concentrate at the outer edges of the strips at the higher frequencies. The odd-mode current distributions in the frequency range considered were all nearly identical, but in this case the current shifted slightly to the inner edges of the strip.

IV. Conclusions

A method has been presented for determining the frequency-dependent characteristics of the dominant mode in microstrip transmission lines. The method can also be extended to calculate the characteristics of higher order modes, and was used to calculate the divergence or cutoff frequencies of several modes. The bulk of the numerical results were presented for microstrip enclosed in a metal box, and the effects of the box size on the characteristics of the line were examined. It was found that reducing the topwall to ground-plane spacing increased the dispersion as a function of frequency, while reducing the spacing between the sidewalls reduced the dispersion. This sidewall effect was correlated to the virtual lack of dispersion for the odd-mode characteristics of coupled lines, while the increase in dispersion with increasing stripwidth was related to the highly dispersive characteristics of the even mode for coupled lines. The even- and odd-mode effective dielectric constants were calculated for several of the compensated structures, and it was shown that the even- and odd-mode phase velocities can be equalized for a particular frequency. The minimum obtainable directivity over an octave bandwidth was shown to decrease as the compensation frequency increases.

The frequency dependence of the impedance for single and coupled lines was also considered, and it was shown that the percent change in impedance from its zero-frequency value is in general less than the corresponding percent change in the effective dielectric constant. Also the results show that the impedance increases as a function of frequency.

References

[1] H. A. Wheeler, "Transmission-line properties of parallel strips separated by a dielectric board," *IEEE Trans. Microwave Theory Tech.*, vol. MTT-13, pp. 172–185, Mar. 1965.
[2] T. G. Bryant and J. A. Weiss, "Parameters of microstrip transmission lines and of coupled pairs of microstrip lines," *IEEE Trans. Microwave Theory Tech. (1968 Symposium Issue)*, vol. MTT-16, pp. 1021–1027, Dec. 1968.
[3] M. K. Krage and G. I. Haddad, "Characteristics of coupled microstrip transmission lines—II: Evaluation of coupled-line parameters," *IEEE Trans. Microwave Theory Tech.*, vol. MTT-18, pp. 222–228, Apr. 1970.
[4] P. Daly, "Hybrid-mode analysis of microstrip by finite-element methods," *IEEE Trans. Microwave Theory Tech.*, vol. MTT-19, pp. 19–25, Jan. 1971.
[5] E. J. Denlinger, "A frequency dependent solution for microstrip transmission lines," *IEEE Trans. Microwave Theory Tech.*, vol. MTT-19, pp. 30–39, Jan. 1971.
[6] J. S. Hornsby and A. Gopinath, "Numerical analysis of a dielectric-loaded waveguide with a microstrip line—Finite difference methods," *IEEE Trans. Microwave Theory Tech.*, vol. MTT-17, pp. 684–690, Sept. 1969.
[7] R. Mittra and T. Itoh., "A new technique for the analysis of the dispersion characteristics of microstrip lines," *IEEE Trans. Microwave Theory Tech.*, vol. MTT-19, pp. 47–56, Jan. 1971.
[8] G. I. Zysman and D. Varon, "Wave propagation in microstrip transmission lines," in *1969 Int. Microwave Symp. Dig.* (Dallas, Tex.), pp. 3–9.
[9] E. J. Denlinger, "Frequency dependence of a coupled pair of microstrip lines," *IEEE Trans. Microwave Theory Tech.* (Corresp.), vol. MTT-18, pp. 731–733, Oct. 1970.
[10] D. Gelder, "Numerical determination of microstrip properties using the transverse field components," *Proc. Inst. Elec. Eng.*, vol. 117, pp. 699–703, Apr. 1970.
[11] R. Pregla and W. Schlosser, "Waveguide modes in dielectric supported strip lines," *Ark. Elek. Übertragung*, vol. 22, pp. 379–386, Aug. 1968.
[12] C. G. Shafer, "Higher mode of the microstrip transmission line," Cruft Lab., Cambridge, Mass., Tech. Rep. 258, Nov. 25, 1957.
[13] M. K. Krage, "Characteristics of microstrip transmission lines," Electron Phys. Lab., Univ. of Michigan, Ann Arbor, Tech. Rep. 122, Nov. 1971.
[14] P. Troughton, "Measurement techniques in microstrip," *Electron. Lett.*, vol. 5, p. 25, Jan. 23, 1969.
[15] L. S. Napoli and J. J. Hughes, "High-frequency behavior of microstrip transmission lines," *RCA Rev.*, vol. 30, pp. 268–276, June 1969.
[16] G. R. Simpson, private communication.